Journal of Electron Spectroscopy and Related Phenomena 195 (2014) 179–184

Contents lists available at ScienceDirect

Journal of Electron Spectroscopy and Related Phenomena

journal homepage: www.elsevier.com/locate/elspec

Spectroscopic investigation of an intrinsic room temperature ferromagnetism in Co doped ZnO nanoparticles

Srinatha N[a], Basavaraj Angadi[a,*], K.G.M. Nair[b], Nishad G. Deshpande[c], Y.C. Shao[c], Way-Faung Pong[c]

[a] Department of Physics, JB Campus, Bangalore University, Bangalore 560056, India
[b] UGC-DAE-CSR, Kalpakkam Node, Kalpakkam, Kokilamedu 603 102, India
[c] Department of Physics, Tamkang University, Tamsui, Taipei 251, Taiwan

ARTICLE INFO

Article history:
Received 4 June 2014
Received in revised form 14 July 2014
Accepted 15 July 2014
Available online 23 July 2014

Keywords:
Dilute magnetic semiconductor
ZnO
L-Valine
SQUID
NEXAFS
XMCD

ABSTRACT

Pure and Co substituted ZnO nano crystalline particles were prepared by solution combustion technique using L-Valine as a fuel. As synthesized powder samples were characterized by X-ray diffractometer and SQUID magnetometer to confirm the formation of single phase wurtzite structure and to study the bulk magnetic response of the sample, respectively. Magnetic studies show that Co doped ZnO nanoparticles exhibit ferromagnetism (FM) at room temperature (RT). Furthermore, the electronic structure and element specific magnetic properties were investigated by near-edge X-ray absorption fine structure (NEXAFS) and X-ray magnetic circular dichroism (XMCD) measurements, respectively. The effect of Co substitution on the spectral features of Co–ZnO at O *K*-edge, Co $L_{3,2}$ edge, Zn $L_{3,2}$ edge have been investigated. The spectral features of NEXAFS at Co $L_{3,2}$ edge is entirely different from the spectral features of metallic clusters and other impurity phases, which rules out the presence of impurity phases. The valence state of 'Co' ion is found to be in +2 state. The FM nature of the sample was confirmed through XMCD spectra, which is due to the incorporation of divalent 'Co' ions. Hence the presented results confirm the substitution of 'Co' ions at 'Zn' site in the host lattice, which is responsible for the RTFM.

1. Introduction

Dilute magnetic semiconductors (DMSs) are the potential candidates for spintronic applications such as spin-polarized information storage and processing devices [1–3]. In order to realize the spintronic devices, the DMS's must exhibit ferromagnetism (FM) at room temperature (RT). Dietl et al. [4] and Sato et al. [5] predicted that, the transition metal ions doped ZnO are the promising candidates for spintronics applications with intrinsic DMS properties at RT. In this context transition metal doped ZnO DMS's are being extensively studied in the form of both nanoparticles [6–10] and thin films [11–17] by various research groups. Co doped ZnO based DMS materials are of great interest, due to the tunability of FM above RT, high solubility limit and large magnetic moment per 'Co' ion. But achieving single-phase, RTFM DMS is relatively difficult due to the formation of 'Co' metallic clusters or other impurity oxide phases. However, theoretical and experimental controversies on the issue of whether magnetism is intrinsic (carrier-induced) or extrinsic (secondary phase formation) are still prevailing. Theoretical calculations by Sako and Katayama-Yoshida [5], have predicted that intrinsic FM of Co doped ZnO can be achieved by electron-doping, when magnetic dopants substituted at 'Zn' cation sites. There are few reports with experimental results on Co doped ZnO with DMS properties [6–17]. But the possibilities of extrinsic FM have not been ruled out, in fact it has been observed in Co doped ZnO [18–21], due to the formation of metallic Co impurity, Co_3O_4 phases and oxygen vacancies. Hence the origin of FM in Co doped ZnO is still under debate and not understood well yet. The near-edge X-ray absorption fine structure (NEXAFS) is an effective experimental tool and is an element specific technique, which can give information about the valance state, local environment, and hybridization of the specific cation (Co) in the material. On the other hand, X-ray magnetic circular dichroism (XMCD) can be used to probe information regarding the contribution of specific cation in any material toward the total magnetism of the system. It is also used to determine the spin and orbital contributions to the magnetism using sum rules [22,23]. In this work, we synthesized Co doped ZnO nanoparticles by solution combustion technique (SCT) using L-Valine as a fuel and

* Corresponding author.
E-mail addresses: brangadi@gmail.com, brangadi@bub.ernet.in (B. Angadi).

http://dx.doi.org/10.1016/j.elspec.2014.07.009
0368-2048/

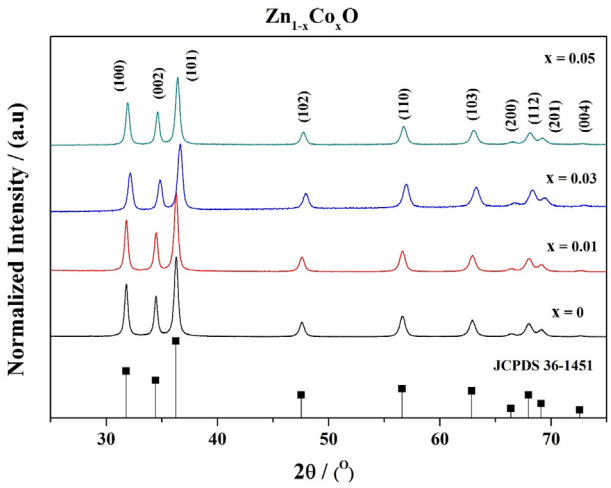

Fig. 1. The XRD pattern of as synthesized $Zn_{1-x}Co_xO$ ($x = 0$, 0.01, 0.03 and 0.05).

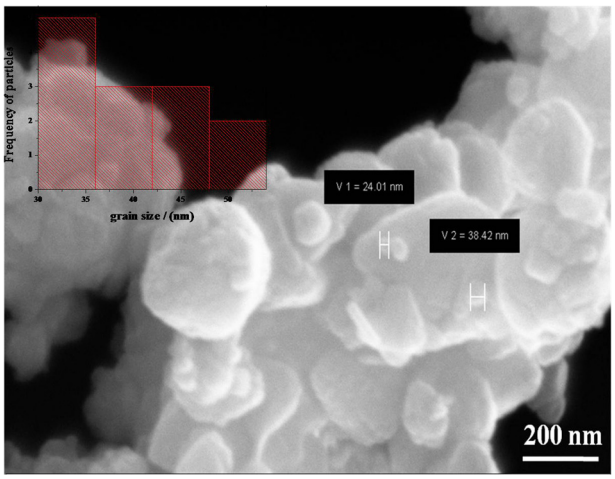

Fig. 2. SEM micrographs of pure ZnO nano powders. Inset shows the distribution of particles (grains).

we report the intrinsic RTFM through NEXAFS and XMCD studies of the Co doped ZnO nanoparticles along with bulk superconducting quantum interference devices (SQUID) magnetic measurements.

2. Experimental

Pure and Co substituted ZnO nanoparticles were prepared by the SCT using Zinc Nitrate Hexa-hydrate as an oxidizer and L-Valine as a fuel and cobaltous nitrate hexa-hydrate as dopant. Stoichiometric amounts of oxidizer (O) and fuel (F) were taken based on the condition that the valance of O/F to be unity, using total oxidizing and reducing valences of the oxidizer and the fuel. These stoichiometric amounts of starting materials dissolved in the double distilled water and stirred completely to get transparent solution. The transparent solution was dried on hot plate/muffle furnace at 100 °C to remove water content in the solution. So obtained sticky solution (water free) was then placed in the pre-heated muffle furnace at 400 °C for combustion process. Within 5 min, the solution ignites fires with flame and finally left with voluminous foamy product (ash). The final foamy product was collected and ground using agate make pestle and mortar.

As-synthesized samples were characterized for phase purity using X-Ray Diffractometer (D8 ADVANCE, Bruker) with wavelength 1.5418 Å and magnetic studies at RT through SQUID magnetometer. Electronic structure and element specific magnetic properties were investigated through NEXAFS and XMCD measurements. X-ray absorption spectroscopy (XAS) i.e., NEXAFS measurements were carried out at different beamlines (BL-11A, 17C and 20A) available at National Synchrotron Radiation Research Center (NSRRC) in Taiwan. Together with SQUID, we also measured the XMCD at 11A1 (Dragon) beamline of NSRRC, Taiwan. All the beamline X-ray absorption data was obtained in the fluorescence yield (FLY) mode, which is mostly bulk sensitive.

3. Results and discussions

To synthesize Co–ZnO nanoparticles, for the first time L-Valine has been utilized as a fuel by SCT. Fig. 1 shows the XRD patterns of pure and Co doped ZnO nanomaterials. From the figure, it is seen that, all peaks could be indexed to the JCPDS card no. 36-1451, belongs to hexagonal wurtzite ZnO phase with space group *P63mc*. It is evidenced from the XRD pattern that as synthesized pure and Co substituted ZnO is in pure single phase, polycrystalline in nature and there is no secondary/impurity phase like, CoO_x, metallic Co, etc. It indicates that, 'Co' ions are substituting 'Zn' ions without any secondary phase formation. A shift in the XRD peaks is observed in Fig. 1, which could be due to the increased substitution of 'Co' cation into 'Zn' site, which leads to change in the lattice parameters or unit cell volume. The Rietveld refinement was carried out on the XRD data using *Fullproof* suite. The refined lattice parameters are tabulated in Table 1. The lattice parameters show small variation with increase of 'Co' doping in ZnO. This could be due to a very small doping concentration (diluted) (<5%) and also could be due to the presence and variation of oxygen vacancies with increase of 'Co' doping. Hence, the variations in lattice parameters are not that significant. These results are in agreement with those reported in literature [24,25].

The crystallite size and strain were calculated using Williamson-Hall Eq. (1).

$$\beta \cos\theta = \frac{k\lambda}{D} + 4\varepsilon \sin\theta \quad (1)$$

where, β is the observed FWHM, θ is the Bragg angle, k is the Scherer's constant, λ is the wavelength of the X-ray used, D is the crystallite size, ε is the strain present in the crystal.

Crystallite size and strain were determined from the intercept and slope obtained by plotting $\beta \cos\theta$ along y-axis and $4 \sin\theta$ along x-axis. The obtained values of crystallite size and strain are tabulated in Table 1. It is seen from the table, the average crystallite size found in the range 20–30 nm. The decrease of crystallite size and the strain as a function of 'Co' concentration were observed and are attributed to the relative difference in the ionic radii of cations ('Co' and 'Zn'). The substitution of 'Co' into 'Zn' site would have altered the geometrical structure of the ZnO, thereby introducing lattice micro strain in the material. The crystallite size of the combustion synthesized material is strongly dependent on the exothermicity of the combustion reaction. In this case the inclusion of Co precursor along with the Zn precursor would have altered the exothermicity of the reaction there by changing the crystallite size.

The micro-structural and surface morphology were studied using scanning electron microscopy. The SEM micrograph of pure ZnO is depicted in Fig. 2. It is seen from the micrograph that, as synthesized samples are agglomerated, porous in nature and particles are uniformly distributed. It is the indicative sign of evolution of large amounts of nitrate gasses during combustion. Though, as synthesized product (powder) is agglomerated, the average particle (grain) size of ZnO particles is found to be in the range of nano regime i.e. 30–50 nm (inset of Fig. 2), it is partial in agreement with the values found from XRD analysis. The particle size distribution is also presented in the form of histogram as an inset in Fig. 2.